Neuron
Article

Role of Olivary Electrical Coupling in Cerebellar Motor Learning

Ruben S. Van Der Giessen,[1,6] Sebastiaan K. Koekkoek,[1,6] Stijn van Dorp,[5,6] Jornt R. De Gruijl,[1,5,6] Alexander Cupido,[1,6] Sara Khosrovani,[1,6] Bjorn Dortland,[1] Kerstin Wellershaus,[2] Joachim Degen,[2] Jim Deuchars,[3] Elke C. Fuchs,[4] Hannah Monyer,[4] Klaus Willecke,[2] Marcel T.G. De Jeu,[1] and Chris I. De Zeeuw[1,5,*]
[1]Department of Neuroscience, Erasmus MC, 3000 DR Rotterdam, The Netherlands
[2]Institute of Genetics, Division of Molecular Genetics, University of Bonn, 53117 Bonn, Germany
[3]Institute of Membrane and Systems Biology, University of Leeds, LS2 9JT Leeds, UK
[4]Department of Clinical Neurobiology, Interdisciplinary Center for Neuroscience, 69120 Heidelberg, Germany
[5]Netherlands Institute for Neuroscience, Royal Academy of Arts and Sciences (KNAW), 1105 BA Amsterdam, The Netherlands
[6]These authors contributed equally to this work.
*Correspondence: c.dezeeuw@erasmusmc.nl
DOI 10.1016/j.neuron.2008.03.016

SUMMARY

The level of electrotonic coupling in the inferior olive is extremely high, but its functional role in cerebellar motor control remains elusive. Here, we subjected mice that lack olivary coupling to paradigms that require learning-dependent timing. Cx36-deficient mice showed impaired timing of both locomotion and eye-blink responses that were conditioned to a tone. The latencies of their olivary spike activities in response to the unconditioned stimulus were significantly more variable than those in wild-types. Whole-cell recordings of olivary neurons in vivo showed that these differences in spike timing result at least in part from altered interactions with their subthreshold oscillations. These results, combined with analyses of olivary activities in computer simulations at both the cellular and systems level, suggest that electrotonic coupling among olivary neurons by gap junctions is essential for proper timing of their action potentials and thereby for learning-dependent timing in cerebellar motor control.

INTRODUCTION

More than a century ago, in 1906, Santiago Rámon y Cajal received the Nobel Prize for the neuron doctrine stating that neurons operate as anatomically and functionally distinct cellular units in the mammalian brain. This tenet still holds, but over the past decade the neuron doctrine has been complemented by new discoveries about the constitution, distribution, and cell-physiological functions of neuronal gap junctions that can establish cytoplasmic continuity among large ensembles of neurons (Bullock et al., 2005). Importantly, in 1998, groups led by Condorelli (Condorelli et al., 1998) and Willecke (Sohl et al., 1998) cloned the first gap junction protein, i.e., connexin36 (Cx36), that is predominantly expressed by neurons. The identification of this protein allowed several groups to study the distribution of Cx36 and/or to create mouse mutants to investigate the cellular consequences of a lack of Cx36 in the brain (Bennett and Zukin, 2004; Connors and Long, 2004). To date, Cx36 and neuronal gap junctions are widely distributed in regions such as the olfactory bulb, hippocampus, cerebral cortex, (hypo)thalamus, and inferior olive (De Zeeuw et al., 1995). For most of these regions, the possible role of neuronal gap junctions has been determined at the cell-physiological level (Deans et al., 2001; Landisman et al., 2002; Long et al., 2002); In these in vitro studies, a lack of Cx36 generally leads to an absence of electrotonic coupling and to changes in subthreshold activities (Long et al., 2002; Buhl et al., 2003; De Zeeuw et al., 2003). Yet, for most of the brain systems mentioned above, the apparent behavioral phenotype is relatively mild and/or remains a topic for systems electrophysiological investigations (Guldenagel et al., 2001; Frisch et al., 2005; Long et al., 2005; but see also Deans et al., 2002, for studies on retina). With regard to the olivocerebellar system, previous behavioral studies on *Cx36*$^{-/-}$ mutants showed no ataxia and a relatively normal motor performance (Kistler et al., 2002). This lack of a clear phenotype during natural motor behavior is remarkable, because in mammals the density of gap junctions in the inferior olive is probably higher than in any other brain region (De Zeeuw et al., 1995). Here, we show that, although *Cx36*$^{-/-}$ mutants have no prominent general motor deficits, they do show problems when challenged to perform a learning-dependent motor task such as conditioning their locomotion pattern or eye-blink response to a tone. In these learning tasks, the timing of the motor responses is modified by conditioning the movement to a conditioned stimulus (CS) that starts before, but coterminates with, an unconditioned stimulus (US) (Perrett et al., 1993; Garcia and Mauk, 1998; Koekkoek et al., 2003). The CS is probably conveyed by the mossy fiber-parallel fiber system to the Purkinje cells in the cerebellar cortex, while the US is conveyed by their climbing fibers originating from the inferior olive (Hesslow et al., 1999; De Zeeuw and Yeo, 2005). Thus, in the current study we investigated the hypothesis that appropriate timing of conditioned motor responses critically depends on the precise temporal coding of the activities of coupled neurons in the inferior olive.

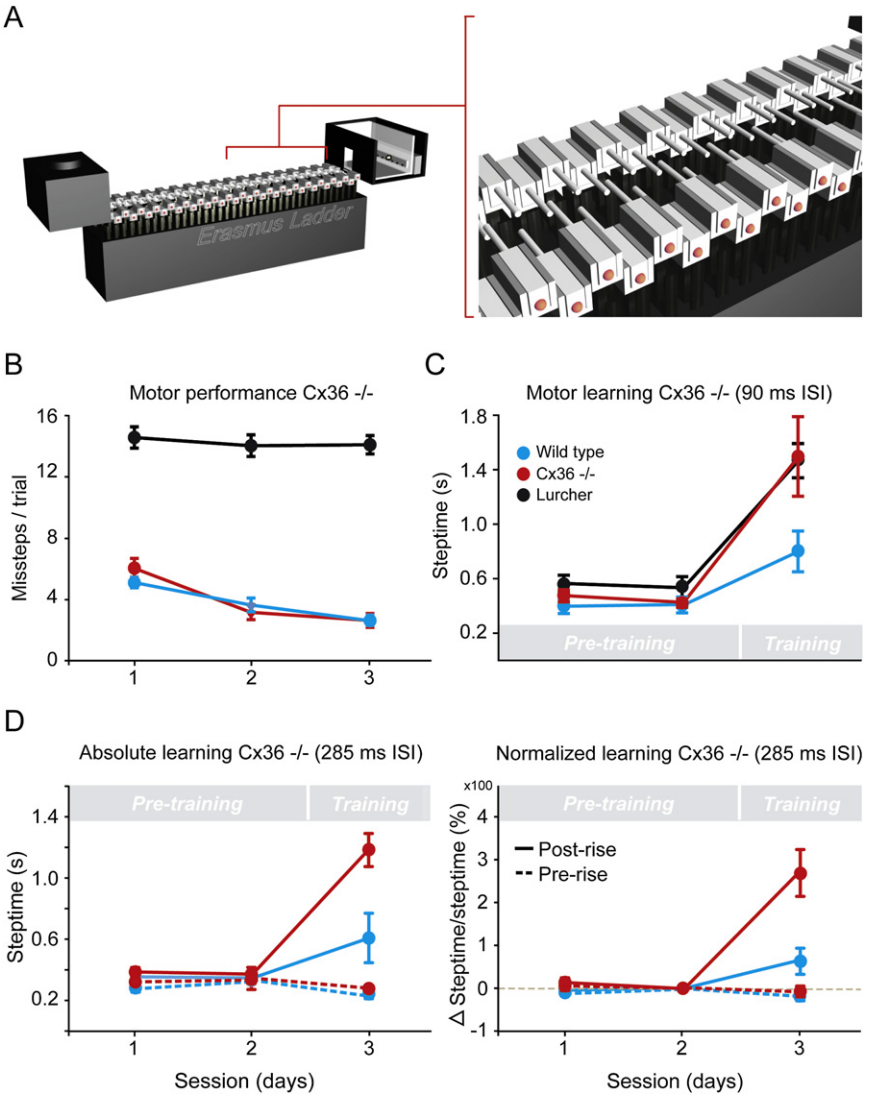

Figure 1. Erasmus Ladder Test for Detecting Performance and Learning Deficits in Locomotion

(A) The ladder consists of 2 × 37 horizontal rungs placed in between two shelter boxes. Mice are trained to walk from one side to the other using air pressure devices placed in the bottom of the boxes. The rungs, which are all equipped with pressure sensors, can be moved up or down under the control of a linked computer system that can analyze the walking pattern instantaneously during locomotion.

(B) Motor performance level is revealed by the amount of descended rungs touched, which represents the number of missteps. *Cx36*$^{-/-}$ mutants (red) and wild-type littermates (blue) show normal motor performance, while *lurcher* mice (black) show deficits in performance during all sessions.

(C) Motor learning level is revealed by the change in steptime after and before conditioning (i.e., training versus pretraining). During conditioning trials, a randomly selected rung rises 12 mm above the walking level to create a perturbation; this unconditioned stimulus occurs at a fixed moment (interstimulus interval [ISI]) after the onset of the conditioned stimulus (a 15 kHz tone). Both *Cx36*$^{-/-}$ mutants and *lurcher* mice reveal difficulties in motor learning.

(D) While the data obtained in (C) have been obtained with an ISI of 90 ms, these data have been obtained with an ISI of 285 ms. Note that the deficits in learning-dependent timing are just as pronounced with this longer ISI, regardless whether they are revealed in an absolute (left) or normalized (right) fashion. The normalized data show values with respect to those obtained in session 1. Also note that the steptimes in the phase preceding the rise of the rung (prerise) are not prolonged during the training (dotted curves). Values indicate mean ± SD.

RESULTS

Deficits in Locomotion Conditioning

To quantify their general level of motor performance, *Cx36*$^{-/-}$ mutants (C57BL/6 background, n = 16) and wild-type littermates (n = 18) were trained to walk on the Erasmus ladder. The Erasmus ladder is formed by 2 × 37 rungs positioned between a start and end box across which the mice can run back and forth (Figure 1A, left panel) (see Supplemental Data section A available online). Each rung on both the left and right side is equipped with a pressure sensor, which is continuously monitored. Based on instantaneous analysis of the activities of these sensors, the walking pattern of the mice can be predicted in the millisecond range and, if wanted, interrupted by moving each individual rung up or down. Initially, the mice were trained with the even-numbered rungs on the left side and the odd-numbered rungs on the right side in a descended position so as to create an alternated stepping pattern with 30 mm gaps (Figure 1A, right panel).

In this paradigm, the *Cx36*$^{-/-}$ mutants and wild-type littermates showed a similar overall average steptime, which was defined as the time needed to place the front paw from one rung to the other (358 ms ± 29 SD for *Cx36*$^{-/-}$ mutants and 339 ms ± 23.5 SD for wild-types), and a comparably low number of missteps, which were identified by touches on the descended rungs ($p > 0.10$ for each session, t test; Figure 1B). For comparison, we also tested *lurcher* mice (C57BL/6 background, n = 9), which lack Purkinje cells and are known to show cerebellar ataxia (Van Alphen et al., 2002; Porras-Garcia et al., 2005). Indeed, these spontaneous mouse mutants showed longer steptimes (589 ms ± 49 SD; $p < 0.01$ in both cases, t tests) and three to four times more missteps than *Cx36*$^{-/-}$ mutants or controls ($p < 0.0001$ and $p < 0.0001$ for each session, t tests). Thus, in line with previous rotarod tests (Kistler et al., 2002; Frisch et al., 2005), we conclude from this test on the Erasmus ladder that *Cx36*$^{-/-}$ mutants show, in contrast to *lurcher* mice, a relatively normal motor performance.

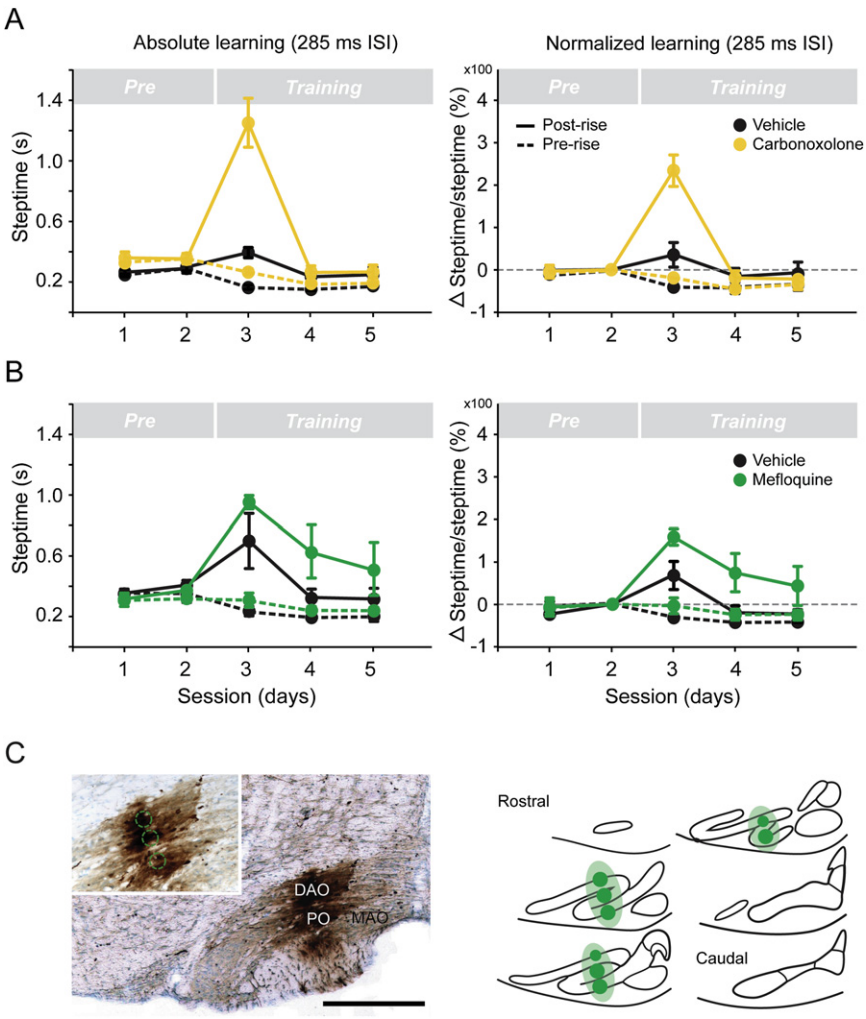

Figure 2. Systemic Applications of Carbenoxolone or Intraolivary Injections of Mefloquine Affect Learning-Dependent Timing

(A) Carbenoxolone was injected i.p. just before the two motor performance sessions (*Pre*) and just before the first of a series of three conditioning sessions (*Training*).

(B) Mefloquine was injected bilaterally inside the inferior olive 1 day before the series of the three conditioning sessions.

(C) Example of one of the reconstructions of the injection site in the olive following BDA labeling. Values indicate mean ± SD.

To find out whether the ability for motor learning is affected in *Cx36*$^{-/-}$ mice, we subjected them to a conditioning paradigm in which they were trained to make a new locomotion movement using a 15 kHz tone as the CS and a rising rung as the US (ISI of 90 ms; see Supplemental Data section A). A training session consisted of eight blocks of eight trials, which were separated by an intertrial interval of 8–12 s. As described above for the initial motor performance test, during the preconditioning sessions, the steptime was not different among mutants and controls ($p > 0.25$, t test). However, as soon as the conditioning procedure started, the front paw steptime in the mutants increased significantly compared to that of controls ($p < 0.05$, t test). In fact, this increase in steptime was comparable to that of *lurchers* (Figure 1C). The difference among mutants and wild-types remained when we prolonged the interstimulus (CS – US) intervals (ISIs) from 90 ms to 285 ms ($p < 0.001$, t test) (Figure 1D).

Because the *Cx36*$^{-/-}$ mutants lack Cx36 from early on and may therefore show compensations within the olivary neurons (De Zeeuw et al., 2003), we also tested the same conditioning Erasmus ladder paradigm in wild-type mice following application of drugs that can block olivary coupling instantaneously (Blenkinsop and Lang, 2006; Martin and Handforth, 2006; Placanonakis et al., 2006; for side effects see Cruikshank et al., 2004; Rozental et al., 2001). We either applied carbenoxolone systemically (40 mg/kg) just before two motor performance sessions and just before the first of a series of three conditioning sessions (n = 5), or we made intraolivary injections with mefloquine (150 μM) 1 day before a series of three conditioning sessions (n = 4) (Gareri et al., 2005; Margineanu and Klitgaard, 2006). In these experiments, we also found a significantly greater increase in the front paw steptime of the coupling-deficient animals after, but not before, conditioning than in control animals (n = 6 and 5, respectively), which received injections with vehicle only ($p < 0.002$ and $p < 0.001$, respectively, t tests) (Figures 2A–2C). In the case of carbenoxolone, the impact of the drug on conditioning tapered off more quickly than that observed after the mefloquine injections (at session four, $p < 0.05$, t test); this difference may be due to a relatively strong and fast clearance of carbenoxolone (Martin and Handforth, 2006; Saffitz et al., 2000).

Taken together, the experiments on the *lurcher* mice and on the animals subjected to intraolivary injections described above showed that the Erasmus ladder allows us to detect specific deficits in both cerebellar motor performance (*lurcher*) and cerebellar motor learning (pharmaceutical manipulation of the olive). We can therefore conclude that genetic or pharmaceutical blocking of olivary coupling mediated by Cx36 has relatively little effect on cerebellar motor performance, while it probably does affect cerebellar motor learning in that the training process is slowed down substantially.

Deficits in Eye-Blink Conditioning

Analysis of the locomotion conditioning process described above suggests that learning-dependent timing is affected in *Cx36*$^{-/-}$ mice. However, in this paradigm, the movements are analyzed in discrete steps, which makes it virtually impossible to identify the exact deficits over time during continuously recorded ongoing locomotion movements. Thus, to further

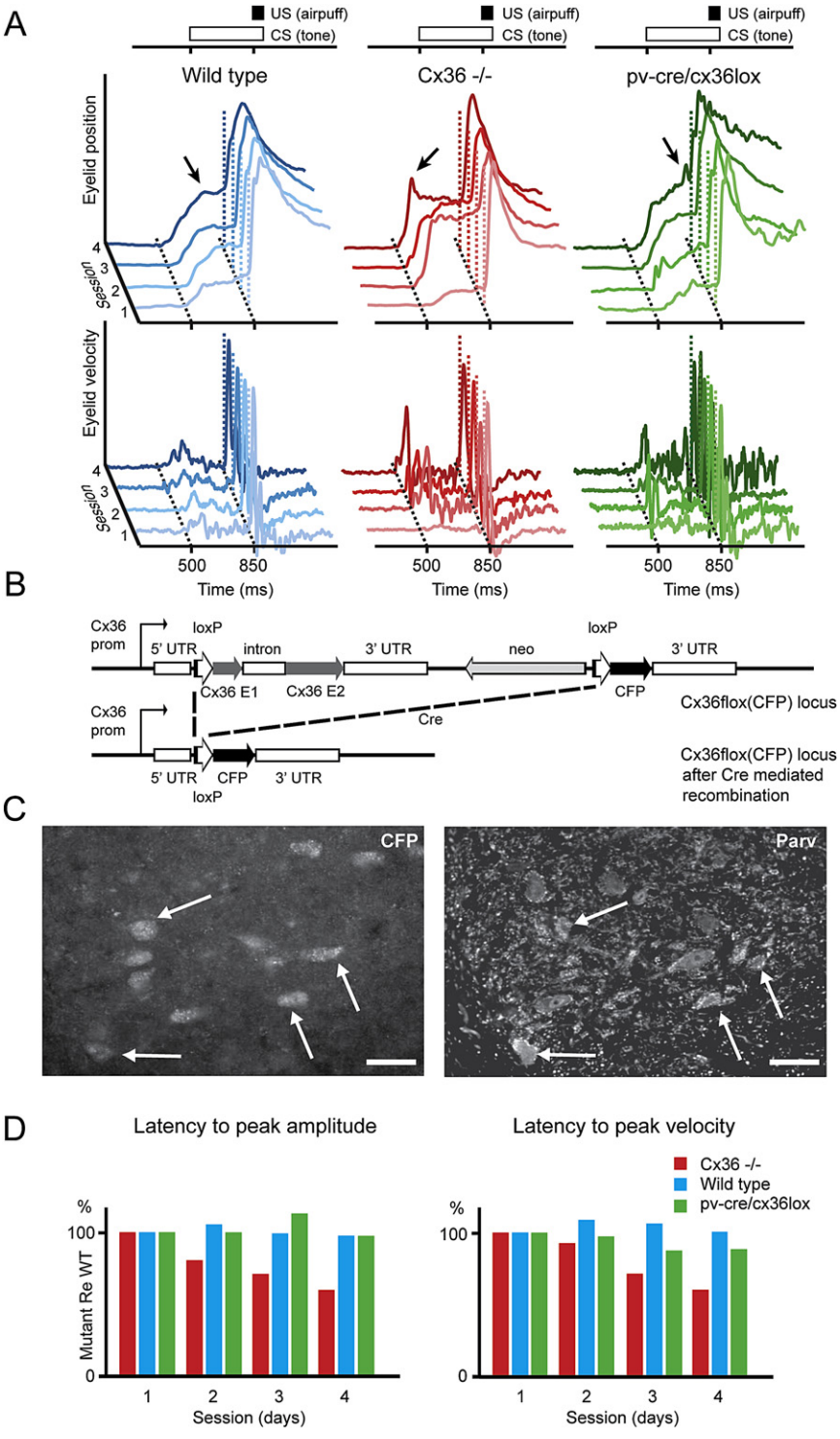

Figure 3. A Lack of Coupling by Cx36 Gap Junction Proteins in the Inferior Olive, but Not in the Cerebellar Nuclei, Results in Impaired Learning-Dependent Timing

(A) Representative examples of eye-blink traces in a wild-type (blue), global *Cx36*$^{-/-}$ mutant (red), and Cx36 del(lacZ)/flox(CFP): parvalbumin-Cre control mouse (green). They all show conditioned eye-blink responses after four training sessions using a tone as the conditioned stimulus (CS) and an air puff as the unconditioned stimulus (US). However, while the timing of the learned response in wild-type and floxed-Cre control mice improves over the sessions, that in the global *Cx36*$^{-/-}$ mutants gets worse (see arrows).

(B) Genetic design of floxed-Cx36 mutants cross-bred with parvalbumin-Cre mice, which were used as controls.

(C) The Cx36 del(lacZ)/flox(CFP): parvalbumin-Cre control mice showed CFP staining in their cerebellar nuclei neurons, demonstrating that Cx36 has been floxed in these neurons and thus not expressed. Immunostaining for parvalbumin of the same sections (right panel) showed that most of the cerebellar nuclei neurons indeed express parvalbumin (arrows) and that they would otherwise in the nonfloxed situation express Cx36. Thus, the Cx36 del(lacZ)/flox(CFP): parvalbumin-Cre control mice do not express Cx36 in their cerebellar nuclei, while their expression in the relevant olivary subnuclei is normal (data not shown). Punctate labeling in neuropil of the right panel reflects staining of axonal fibers.

(D) While the latency to peak amplitude (left panel) in the global knockouts of Cx36 (red) got worse during the training sessions, that in the Cx36 del(lacZ)/flox(CFP): parvalbumin-Cre control mice (green) was indistinguishable from that in their unaffected littermates (blue). Similarly, the average latency to peak velocity (right panel) in the mutants was also significantly reduced ($p < 0.01$; t test).

investigate the potential role of Cx36 in learning-dependent timing, we compared the *Cx36*$^{-/-}$ mutants with wild-type littermates in an eye-blink conditioning paradigm. For this paradigm, the motor responses can be continuously measured using the magnetic distance measurement technique (MDMT; Koekkoek et al., 2002). We subjected adult *Cx36*$^{-/-}$ mutants (n = 8) and wild-type littermates (n = 8) to a conditioning paradigm using a tone as the CS and an air puff as the US at ISIs of 350 ms. Here, too, the eight daily training blocks consisted of eight trials (one US alone, six paired, and one CS alone). After four paired training sessions (T-1 to T-4), the percentage of conditioned responses and their average peak amplitude in wild-types reached levels of 77% and 0.48 mm, respectively, while those in *Cx36*$^{-/-}$ mice had values of 78% and 0.56 mm. These values were not significantly different ($p > 0.9$ and $p > 0.5$; MANOVA). In contrast, the timing properties of the conditioned responses differed dramatically among wild-types and mutants as the training proceeded. While in wild-types the average latency to peak amplitude of the conditioned responses was appropriately fixed at the moment when the US occurs, the timing in mutants got worse during the four training sessions (Figure 3A

and Supplemental Data section B). At the end of the training, the average latency to peak amplitude in the mutants preceded the moment of the US by 196 ms (±27 SD), which was significantly different from that in controls (80 ms ± 24 SD; $p < 0.005$, t test) (see also Figure 3D). These data indicate that coupling-deficient mutants cannot appropriately time their movements when challenged in a conditional task.

Still, these eye-blink experiments on the global Cx36 null mutants do not directly demonstrate that the behavioral phenotype can be attributed solely to a lack of coupling in the inferior olive. GABAergic neurons in many brain regions, including those in the cerebellar nuclei, also show a prominent expression of Cx36 (Degen et al., 2004; Van Der Giessen et al., 2006), and a lack of this expression may therefore in principle also affect cerebellar conditioning. To address this potential caveat, we generated mutant mice in which the expression of Cx36 is ablated in the GABAergic neurons of the brain, while that in the relevant olivary neurons, which are all non-GABAergic, is normal (Figures 3B and 3C). These mutants (n = 4), which were cross-breedings of floxed-Cx36 mutants and parvalbumin-Cre mice, lacked expression of Cx36 in, for example, the GABAergic neurons of the thalamus, olfactory bulb, cerebral cortex, hippocampus, and cerebellar nuclei that express parvalbumin (Seto-Ohshima et al., 1989), whereas the neurons in the dorsal accessory olive that are involved in eye-blink conditioning showed a normal level of Cx36. The pv-cre/cx36lox cross-bred mutants showed the same conditioned responses as wild-types, i.e., without any deficits in their timing (Figures 3A and 3D). These data indicate that in the global $Cx36^{-/-}$ knockout it is most likely the deficits in the olive that are responsible for the abnormalities in learning-dependent timing. For the same argument, it is also relevant to find out whether coupling among stellate cells in the cerebellar cortex is affected in the Cx36 mutant mice (Mann-Metzer and Yarom, 1999). We therefore investigated the constitution of the gap junctions between these cells. It turned out that the vast majority of these interneuronal gap junctions are formed by connexin45 (see Figure 5 in Van Der Giessen et al., 2006) rather than Cx36 (Van Der Giessen et al., 2006). Thus, we conclude that $Cx36^{-/-}$ mutants show deficits in learning-dependent timing and that this behavioral deficit is likely due to an impairment of electrotonic coupling in the inferior olive.

Abnormal Temporal Pattern of Climbing Fiber Responses

If the deficits in learning-dependent timing are due to a lack of coupling between the olivary neurons, one would expect that the timing properties of the activities in these neurons would be disrupted in $Cx36^{-/-}$ mutants. To investigate these properties, we recorded the climbing fiber activities of Purkinje cells in the cerebellar cortex that reveal the olivary signals of the US during eye-blink conditioning (Mauk et al., 1986; Hesslow, 1994). The climbing fiber activities of Purkinje cells, also called complex spikes, generally reflect the temporal coding of olivary neurons rather precisely, because they are generated in an all-or-none fashion (De Zeeuw et al., 1998). We found that the Purkinje cells that respond well to air puff stimulation are in the mouse situated in an area covering both lobulus simplex in the hemisphere and the adjacent part of lobule VI in the posterior lobe (Figure 4A). In awake wild-types (n = 9), the air puff stimulation evoked virtually only short-latency climbing fiber responses; these responses had an average peak latency of 29 ± 9 ms (SD, averaged over the nine animals) over 879 successful stimulations (>70% successful). In contrast, in all Purkinje cells recorded in the $Cx36^{-/-}$ mutants (n = 10), the same perioribital stimulation evoked both short-latency responses (average to peak of 30 ± 7 ms) and long-latency responses (101 ± 17 ms) (Figure 4B). Of all successful stimulations (n = 1036, >75% successful) in the mutants, 60% and 34% resulted in pure short-latency and pure long-latency responses, respectively, while 6% resulted in both a short-latency and long-latency response. These differences in the temporal distribution patterns following peripheral stimulation were highly significantly different among wild-types and mutants ($p < 0.001$, t tests). Similarly, during spontaneous activity in the awake state, the $Cx36^{-/-}$ mutants showed significantly ($p < 0.01$, t test) more doublets of two or three climbing fiber responses occurring within 200 ms (12% ± 6%, SD) than wild-types (5% ± 2%, SD) (Figure 4C, upper panel), while their mean interspike interval within a doublet was significantly smaller (123 ± 11 ms in $Cx36^{-/-}$ mutants versus 140 ± 12 ms in wild-types; $p < 0.01$, t test) (Figure 4C, middle panel). This difference was also reflected by a generally increased coefficient of variation for spike intervals ($p < 0.02$, t test) (Figure 4C, bottom panel). All these differences in complex spike activities were not influenced by differences in average firing frequencies, because the average complex spike frequency was not significantly different among wild-types and $Cx36^{-/-}$ mutants (0.94 ± 0.19 versus 1.00 ± 0.26; $p > 0.4$, t test; cf. Marshall et al., 2007, for differences in anesthetized state). Likewise, the shape of the climbing fiber responses and the average number of spikelets within the complex spikes (Figure 4B) as well as the average firing rate (67 ± 13 versus 69 ± 14) and coefficient of variation (0.68 ± 0.2 versus 0.57 ± 0.2) of simple spike activities of the mutants were also not different from those in wild-types. Thus, Purkinje cells in awake mice lacking Cx36 show robust differences in the temporal pattern of their climbing fiber responses, but not in the average firing frequencies of their ongoing activities.

Altered Correlation between Spiking Activities and Subthreshold Oscillations

To explain the differences in latencies and spiking patterns, we investigated the activities of olivary neurons using whole-cell recordings in vivo in anesthetized animals (Table 1). The majority of the neurons in wild-types showed pronounced subthreshold oscillations that either had a clear sinusoidal appearance, a more complex rhythmic shape, which probably corresponds to the activation of low-threshold calcium conductances (Llinas and Yarom, 1981), or both types of subthreshold activities (Figure 5A) (see also Khosrovani et al., 2007). In the mutants, the same types of oscillating cells were observed, but they showed significantly more cells that did not oscillate ($p < 0.01$, χ^2 test), and the occurrence of their oscillations depended significantly stronger on the membrane potential ($p < 0.01$, t test), as previously described for in vitro conditions (Long et al., 2002; De Zeeuw et al., 2003) (Figures 5B and 5C). Power spectra of the oscillating subthreshold activities showed that the frequencies of the oscillations occurred in both wild-types and mutants

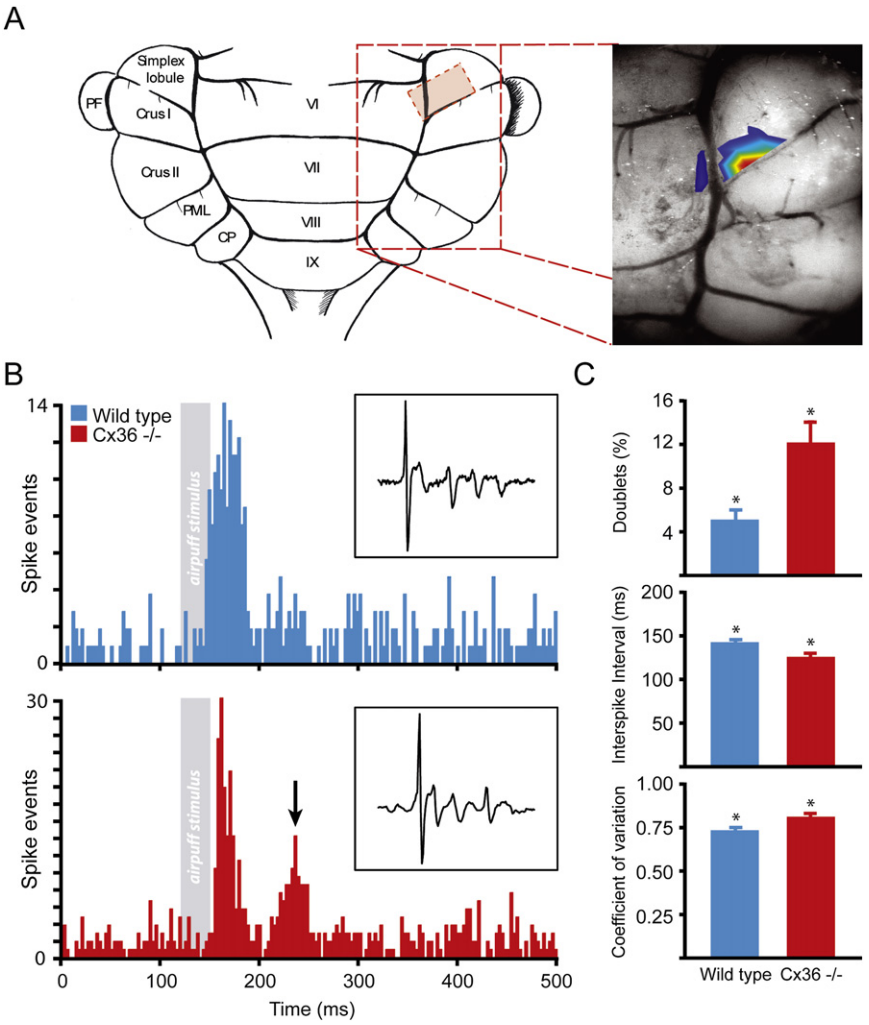

Figure 4. A Lack of Coupling of Inferior Olivary Neurons Results in Altered Timing of Climbing Fiber Activities in the Cerebellar Cortex

(A) Purkinje cells that responded well to air puff stimulation (i.e., US) were situated in an area covering the lobulus simplex in the hemisphere and adjacent part of lobule VI in the posterior lobe. Color codings correspond to percentage of Purkinje cells that responded with complex spike activities to air puff stimulation; red, yellow, green, light blue, and dark blue indicate success rates of 50%, 40%, 30%, 20%, and 10%, respectively.

(B) Air puff stimulation evoked only short-latency climbing fiber responses in awake wild-type mice (blue) (latency of 29 ± 9 ms), while in the *Cx36*$^{-/-}$ mutants (red) the same perioribital stimulation evoked both short-latency (30 ± 7 ms) and long-latency responses (101 ± 17 ms) (arrow). Note that in both cases units on the y axis represent two spikes. Insets show typical complex spike responses in wild-types (top) and mutants (bottom) in 8 ms trace; no differences were observed in the shape.

(C) During spontaneous activity in the awake state, the *Cx36*$^{-/-}$ mutants showed significantly more doublets of two or three complex spikes occurring within 200 ms ($p < 0.01$, t test), a significantly smaller mean interspike interval within these doublets ($p < 0.01$, t test), and a general increased coefficient of variation for spike intervals ($p < 0.02$, t test). Values indicate mean ± SD.

mostly in the range of 1–3 Hz or in the range of 6–9 Hz (Figure 5D). Similarly, action potentials of olivary cells in both wild-types and mutants showed a so-called capacity to reset the subthreshold oscillation (see also Leznik et al., 2002; Leznik and Llinas, 2005; Khosrovani et al., 2007). Still, the olivary activities differed in that the oscillations of the wild-type neurons often showed dynamic crescendo amplitudes starting directly after the generation of an action potential (crescendo amplitudes were defined as at least a 3-fold increase of the amplitude over five cycles), while those in the mutants showed significantly more ($p < 0.05$, t test) constant amplitudes (Figure 5A). Moreover, the relationship between the preferred frequencies of the subthreshold oscillations and those of the olivary spiking activities was less tight in the Cx36 null mutant (mean residual scores of 1.33 versus 0.63; $p < 0.01$, t test) (Figure 5D). Interestingly, this reduced correlation is in line with the observation that the olivary spikes occurred significantly more often ($p < 0.05$, t tests) during the peak period of an oscillation in wild-types than in mutants (peak period is defined as the period plus or minus 90° from the peak) (right panel in Figure 5C; see also arrows in Figure 5A). These differences in interactions between spike generation and subthreshold oscillations also occurred following peripheral stimulation as used in the conditioning paradigms described above (Figure 5E). Following peripheral stimulation, the frequency of the subsequent oscillations in the mutant cells was significantly less stable ($p < 0.02$, t test) than in the wild-types (for quantification of first four cycles after stimulus see Figure 5F). Thus, peripheral sensory stimulation can indeed induce and modify the subthreshold activities, and such modulation can influence the timing of subsequent spiking activities of olivary neurons when they are appropriately coupled. Therefore, the altered timing of the climbing fiber signals mediating the US in the coupling-deficient *Cx36*$^{-/-}$ mutants can at least in part be explained by altered interactions with their subthreshold oscillations.

How May a Lack of Coupling among Olivary Neurons in the *Cx36*$^{-/-}$ Mutant Lead to Altered Spiking?

If the lack of coupling between olivary neurons indeed leads to altered timing of their action potentials due to altered interactions with their subthreshold oscillations, we should be able to find similar relations and characteristics in a simulation of olivary neurons. To this end, we used a modified version of a two-compartmental olivary cell model by Schweighofer et al. (1999) (Figure 6 and Supplemental Data section C including videos). Because direct responses to depolarizing pulses in the olive are generally not delayed for periods of time near 100 ms (Simpson et al.,

Table 1. Properties of Olivary Neurons in Wild-Type and *Cx36*$^{-/-}$ Mutants following Whole-Cell Recordings In Vivo (Values Indicate Mean ± SEM)

Parameter	Wild-Type	n	*Cx36*$^{-/-}$	n	Statistics
Cells Expressing Spontaneous STOs					
Resting membrane potential (mV)	−55 ± 1	53	−55 ± 1	16	0.31
Input resistance (MΩ)	40.1 ± 3.8	53	45.2 ± 4.3	14	0.24
Membrane capacitance (pF)	188.7 ± 11.8	53	233.0 ± 37.0	14	0.07
Firing rate (Hz)	0.64 ± 0.05	50	0.54 ± 0.09	14	0.15
Coefficient of variation for spike intervals	0.72 ± 0.02	50	0.83 ± 0.05	14	0.02
STO frequency (Hz)	3.1 ± 0.3*	53	3.4 ± 0.6*	16	0.32
STO amplitude (mV)	8 ± 1*	53	8 ± 1*	16	0.44
% Cells expressing depolarizing sag	24	58	62	14	0.01
% Cells expressing rebound depolarization	62	58	92	14	0.05
% Cells expressing afterhyperpolarization	19	45	45	12	0.26
Cells Expressing No Spontaneous STOs					
Resting membrane potential (mV)	−52 ± 2	9	−58 ± 1	12	0.11
Input resistance (MΩ)	42.3 ± 5.2	9	48.3 ± 15.5	12	0.32
Membrane capacitance (pF)	159.6 ± 19.1	9	100.6 ± 3.9	12	0.07
Firing rate (Hz)	0.54 ± 0.11	9	0.92 ± 0.35	12	0.10
Coefficient of variation for spike intervals	0.68 ± 0.13	9	0.68 ± 0.04	12	0.49
% Cells expressing depolarizing sag	0	8	0	12	1.00
% Cells expressing rebound depolarization	60	8	100	12	0.29
% Cells expressing afterhyperpolarization	40	8	0	12	0.29

Statistics: t test or χ^2 test. *All measured subthreshold oscillations (STOs); a single cell can have multiple STO frequencies.

1996; Khosrovani et al., 2007), while long-latency responses due to reverberating loops can be readily found when the network is affected (Ruigrok and Voogd, 1995; De Zeeuw et al., 1998), the secondary response found in Cx36-deficient mice is probably caused by another input. Therefore, we applied to both the normal and coupling-deficient situation depolarizing currents timed ~100 ms apart, of which the second was assumed to be caused by a reverberating loop. In both wild-type and *Cx36*$^{-/-}$ mutant cells, the modeled reverberating loop stimulation was in itself, i.e., without the priming induced by the first input, never strong enough to generate an action potential.

The single-cell behavior of the model closely resembled that of its biological counterpart as described in the current and previous work (De Zeeuw et al., 2003). Both cell models oscillate at ~9 Hz, have preferred firing windows on the upward slopes of subthreshold oscillations, exhibit differentially damped oscillations after an action potential, and undergo a phase change (resetting effect) upon stimulation (Figure 6A). The Cx36-deficient cells exhibited subthreshold oscillations with a slightly larger amplitude than that of the wild-type cells and had an increased chance of generating doublets (12% instead of 0% in simulated wild-types). Due to dendritic leak currents, the wild-type cells were less excitable and had smaller firing windows.

In the multiple-cell simulations, electrotonic coupling allowed the ensembles of wild-type cells to gradually build up a charge as pulses come in and to synchronize their action potentials on the first input (Figures 6B and 6C, left panels) (see also video in Supplemental Data section C). Still, the coupled wild-type neurons did not respond to the reverberant input. In contrast, the *Cx36*$^{-/-}$ network depended on increased excitability to be able to respond with at least some level of synchrony, reacting as quickly as possible as pulses to different cells arrive in presumably rapid succession (Figure 6B, right panel). Simulations of Cx36-deficient networks showed a dual response as the reverberating loop stimulation was in this case sufficiently effective (Figures 6B and 6C, right panels). Thus, when the first input arrived outside the firing window, the second pulse could elicit a response in an uncoupled cell, but not in coupled cells (Figure 6C) (videos in Supplemental Data section C). Due to the rebound spikes, dual responses, and a wide spread in timing of the action potentials in the Cx36-deficient cells, the subthreshold oscillations of ensembles of these cells did not synchronize, despite single-cell resetting effects. As a result, the variance in timing of these networks' responses remained high.

How May Altered Spiking Patterns Lead to Changes in Learning-Dependent Timing?

Our data on evoked climbing fiber activities as well as the model of olivary activities indicate that the temporal firing patterns of olivary cells are destabilized when they are not coupled. Considering that coupling of olivary neurons by Cx36 gap junctions also synchronizes climbing fiber activities of ensembles of Purkinje cells within the same parasagittal zone (Marshall et al., 2007; but cf. Kistler et al., 2002), one can appreciate that the overall defect in the temporal patterns of complex spike activities within the olivocerebellar modules must be substantial. To find out how impaired synchrony of climbing fiber responses may lead

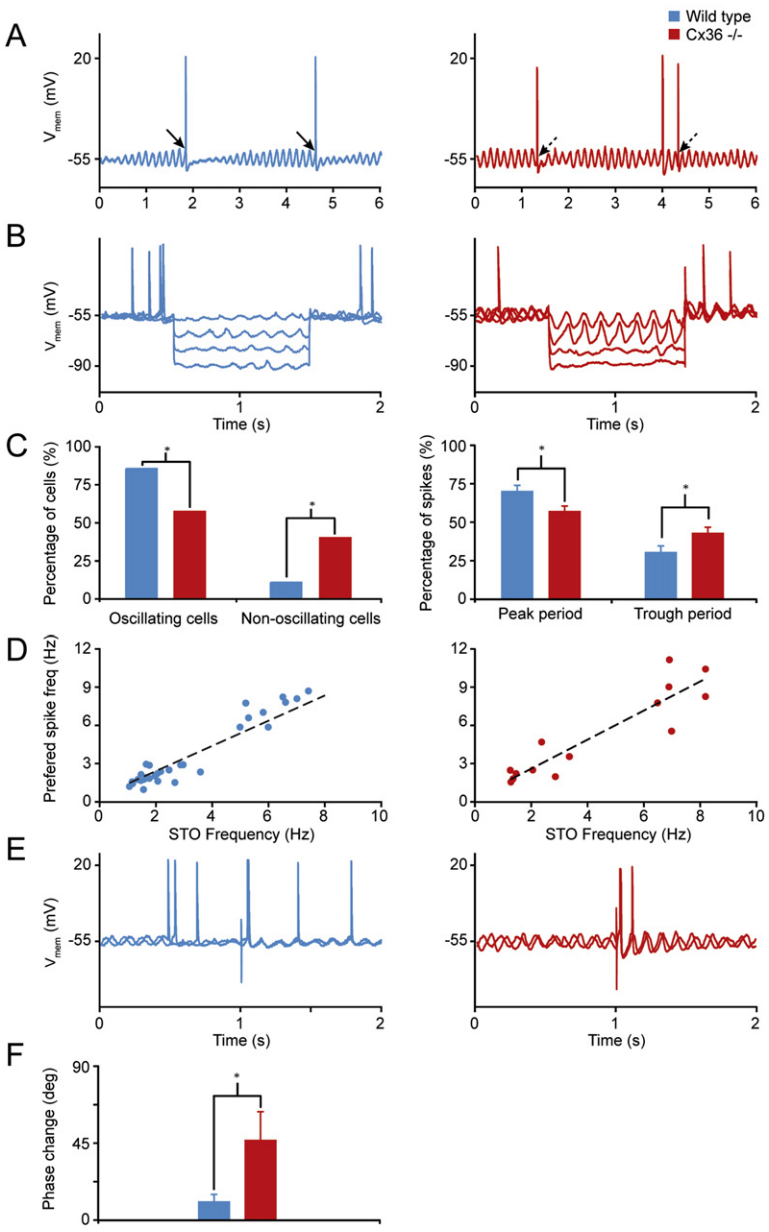

Figure 5. A Lack of Electrotonic Coupling in the Inferior Olive Results in Altered Interactions between Subthreshold Oscillations and Generation of Spiking Activities

(A) Examples of whole-cell recordings of olivary neurons in a wild-type (blue) and *Cx36*$^{-/-}$ mutant (red) in vivo. Most of the olivary spikes in the wild-type occurred around the peak of the oscillations (solid arrows), while those in the mutant frequently also occurred in the trough area (dashed arrows).

(B) Subthreshold oscillations also occurred during hyperpolarizing steps (100 pA) in both wild-types and mutants; however, the oscillations in the mutants depended more strongly on the membrane potential.

(C) (Left panel) Percentages of oscillating and nonoscillating cells differed significantly among wild-types and *Cx36*$^{-/-}$ mutants; *$p < 0.01$ (χ^2 test). (Right panel) When oscillating, the percentage of spikes that occurred in the peak period was significantly lower in *Cx36*$^{-/-}$ mutants, while that in the trough period was significantly higher ($p < 0.05$, t tests). These periods are defined as the peak amplitude plus or minus 90° and the trough amplitude plus or minus 90°, respectively. Percentages indicated are mean values, while error bars indicate SD.

(D) Power spectra showed that the frequencies of both the oscillations and spikes occurred in both wild-types and mutants mostly in the range from 1 to 3 Hz and from 6 to 9 Hz. However, the correlation between the preferred frequency of the oscillations and that of the spiking activities was significantly stronger in wild-types ($p < 0.01$, t test).

(E) Examples of action potentials and subthreshold oscillations in wild-types (left) and *Cx36*$^{-/-}$ mutants (right) before and after peripheral stimulation. In both types of animals, the peripheral stimulation had a resetting effect in that the oscillations after the occurrence of the stimulus were in phase with each other, while they were out of phase before the oscillations. However, while the phase of the subthreshold oscillation remained stable in the wild-type, that in the mutant was unstable. Stimulus artifacts are set at 1.

(F) The average phase change within the first four cycles of ten different traces of an individual cell following peripheral stimulation was significantly greater in *Cx36*$^{-/-}$ mutants than in wild-types ($p < 0.02$, t test; error bar indicates SD).

to deficits in learning-dependent motor timing, we created and tested a model of the olivocerebellar system controlling conditioned responses (Figure 7 and Supplemental Data section D). The model is in line with the hypothesis that plasticity associated with learning a conditioned eye-blink response is distributed among the cerebellar cortex and cerebellar nuclei, which may encode the timing of the response and store a representation of the amplitude of the response, respectively (Koekkoek et al., 2003; Mauk and Donegan, 1997; Perrett et al., 1993; Raymond et al., 1996). Because a functioning cerebellar cortex has been shown to be required for the acquisition and expression of a well-timed conditioned response (Perrett et al., 1993), the inability of Cx36-deficient mice to learn an appropriately timed eye-blink response might be partly due to incorrect guidance of plasticity in the cerebellar cortex, which is known to be under climbing fiber control (Coesmans et al., 2004). We therefore investigated the possibility of a causal link between absence of properly synchronously timed climbing fiber activities and impaired cortical plasticity in a network model of an olivocerebellar module. The model initially analyzes the stability of the strengths of parallel fiber to Purkinje cell synapses during periods when active learning is not taking place and when plastic changes of synaptic strengths may occur due to uncorrelated parallel fiber and climbing fiber background activity. Subsequently, the impact of synaptic instability is explored in the situation when associative conditioning occurs, as postlearning (in)stability of parallel fiber synaptic strength might be directly related to the retention of cortical memory. The following basic assumptions form the guiding principles of the model: (1) the olivocerebellar system is topographically organized, with Purkinje cells, neurons of the cerebellar nuclei, and neurons of the inferior olive connected in discrete closed-loop modules in which the Purkinje cells

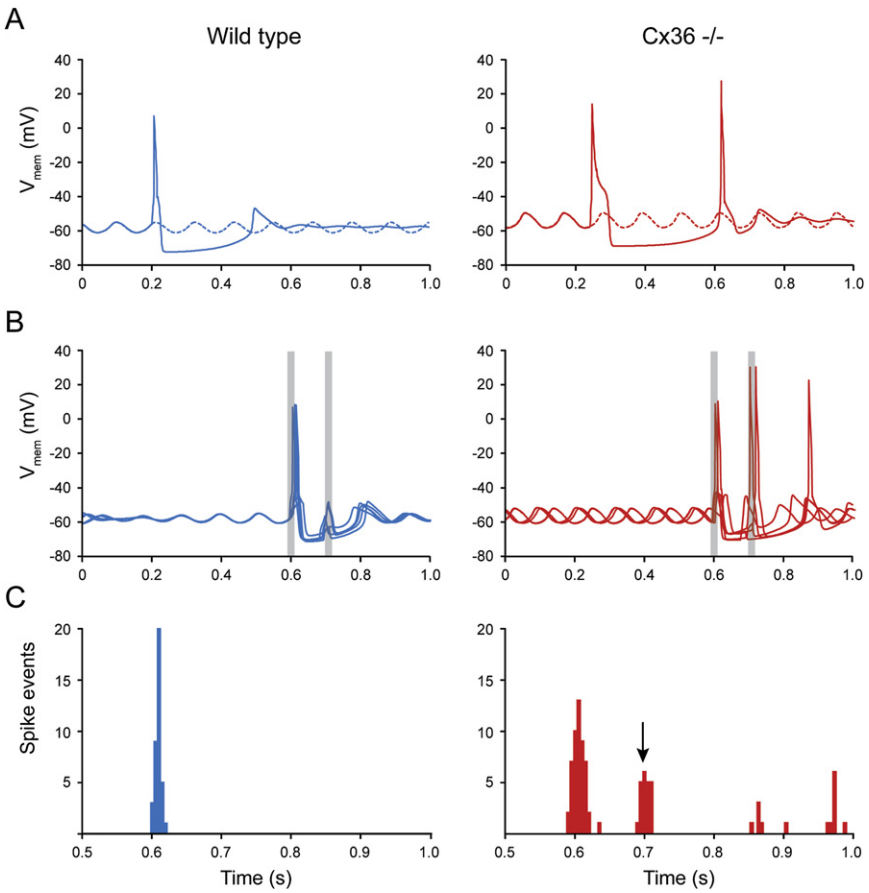

Figure 6. Simulations of Wild-Type (Left Panel; Blue) and Cx36 Knockout (Right Panel; Red) Inferior Olivary Cells Using a Two-Compartmental Computational Model

(A) 1000 ms trace of a wild-type cell and a Cx36-deficient cell. Five $\mu A/cm^2$ depolarizing currents are applied for 15 ms. The wild-type cell generates a spike and shows temporarily damped oscillations afterward. The Cx36-deficient cell responds with a doublet, despite the fact that stimulation occurred in the trough.

(B) Five traces of 1000 ms from one of the wild-type cell ensemble simulations and a Cx36-deficient cell simulation. Due to the random initialization and coupling, the subthreshold oscillations in the wild-type cells are damped at first and increase in amplitude as they become more synchronized (compare with Figure 5A). Two depolarizing 15 ms currents (gray bars) are applied at 600 ± 10 ms (SD) (4.5 $\mu A/cm^2$) and 700 ± 10 ms (SD) (2.5 $\mu A/cm^2$). Exact onset of the currents was randomly determined per cell. The spike responses of the wild-type cells occur in a narrow time window, and the second input does not give rise to any action potentials. Thus, the wild-type network retains its synchronized oscillations. In contrast, due to a lack of coupling, the Cx36-deficient cells do not synchronize their oscillations. Their spike responses are not timed closely together, the second pulse also gives rise to action potentials, and doublets occur. Because of these factors, the Cx36-deficient network does not synchronize.

(C) Temporal distribution of spikes in the wild-type and Cx36-deficient networks. The first depolarizing current was applied at 600 ± 10 ms and the second at 700 ± 10 ms. The coupled wild-type networks synchronize the first volley of spikes and do not respond to the second pulse. In the Cx36-deficient network, the first band consists of approximately the same number of spikes as the wild-type response indicated above, but due to a lack of coupling, the spikes are not as synchronized. Because of the increased excitability, Cx36-deficient cells also exhibit responses to the second pulse and an increased number of doublets.

converge onto the nuclei (Voogd and Glickstein, 1998) (Figure 7A); (2) the strengths of parallel fiber to Purkinje cell synapses can reversibly increase or decrease, depending, for each activated granule cell, on the width of the time interval to the climbing fiber stimulus (Coesmans et al., 2004; Wang et al., 2000); and (3) neurons tend to be more active as their excitatory inputs increase and less active as their inhibitory inputs increase (Kenyon et al., 1998; Medina and Mauk, 2000).

Based upon these general assumptions, one can deduce that adaptive changes of synaptic strengths within the olivocerebellar feedback loop can provide feedback to control activity in the inferior olive around a stable equilibrium value (Kenyon et al., 1998) and that such equilibrium in activities of olivary neurons may in turn be necessary for synapses in the loop to remain stably fixed at their current strength. In the cerebellar loop, it is probably not directly possible for a Purkinje cell to provide a one-to-one feedback to its own climbing fiber, due to the strong convergence of Purkinje cells onto deep cerebellar nuclei neurons (Figure 7A). To enhance the efficiency of this feedback, specific sets of olivary neurons may be selectively coupled. In other words, selective coupling of olivary neurons, which together innervate the complete microzone of the Purkinje cells that converge onto the cerebellar nuclei neurons that provide the GABAergic input to the very same olivary neurons, can stabilize the activities in an entire olivocerebellar module.

Thus, the model shows how gap junction coupling in the olive could help to stabilize the weights of parallel fiber to Purkinje cell synapses by synchronizing climbing fiber feedback to Purkinje cells (Figure 7B). When the activity of olivary neurons is not synchronized, as is the case in Cx36-deficient mutants, incorrect feedback through the cerebellar loop causes parallel fiber to Purkinje cell synaptic strengths to drift and finally saturate at their minimum or maximum strengths (Figures 7C and 7D). Such impairment in induction and maintenance of cortical plasticity in turn can lead readily to a rectangular "amplitude" response in the nuclei, which prevents an optimal closure of the eyelid at the moment when the unconditioned stimulus is about to take place (Figure 7E; compare to Figure 3A).

DISCUSSION

Revealing the electrophysiological mechanisms that underlie the behavioral phenotypes of Cx36-deficient animals remains a topic of intense investigations (Deans et al., 2001; Kistler et al., 2002; Landisman et al., 2002; Buhl et al., 2003; Bennett and Zukin, 2004; Connors and Long, 2004; Placantonakis et al., 2004;

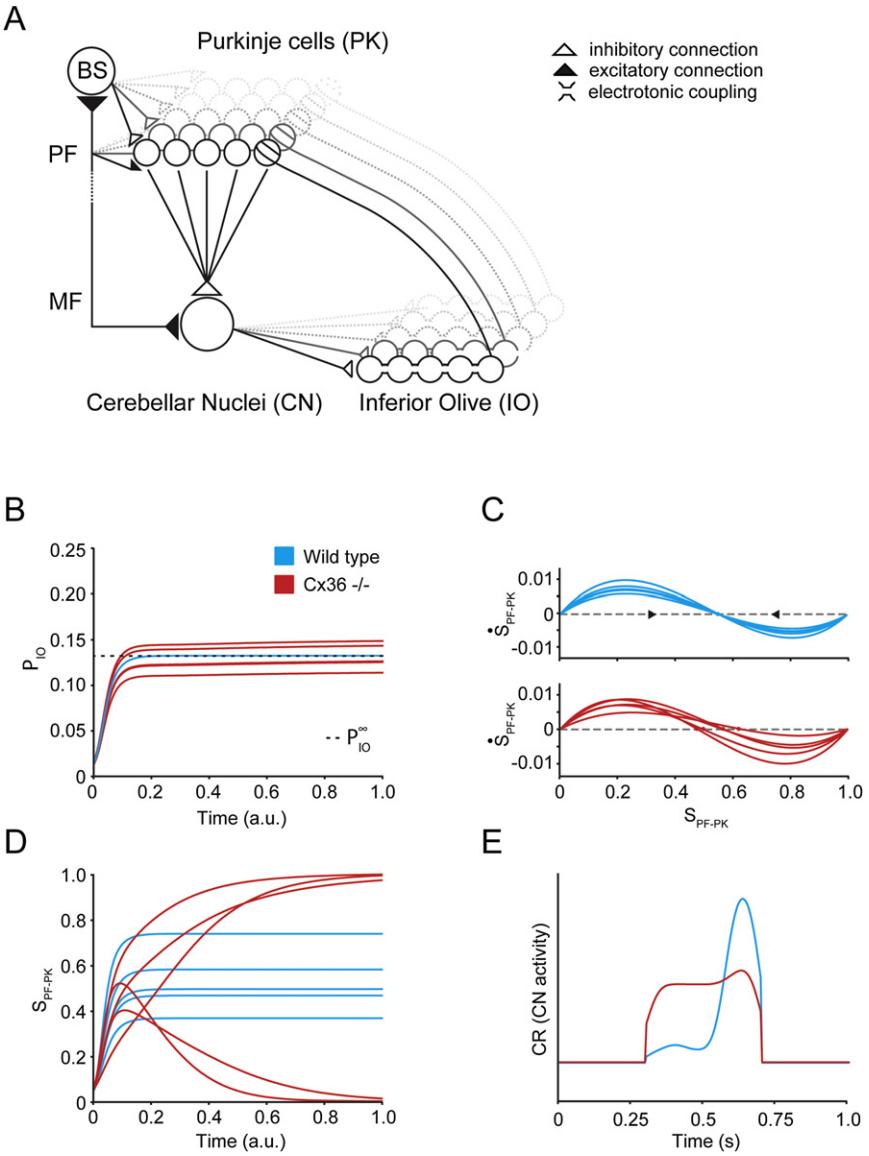

Figure 7. Impact of Altered Olivary Coupling and Spiking on Learning-Dependent Timing in a Network Simulation

For panels (A)–(D), a mathematical model was used to analyze the stability of parallel fiber to Purkinje cell synapses as a function of the average background spike probabilities of parallel fibers and climbing fibers. Panel (E) displays results from a real-time simulation, which incorporates the findings of the mathematical model in a conditioning paradigm. In the simulations, synaptic weights are adjusted according to coincidence rules for parallel fiber and climbing fiber activity. Neural spike probabilities are represented as linear sums of inhibitory and excitatory synaptic inputs, which are defined as the product of presynaptic average activity and synaptic strength. (A) Connectivity within a cerebellar module; Purkinje cells (PK), neurons of the cerebellar nuclei (CN), and neurons of the inferior olive (IO) form a closed loop. A key feature is the strong convergence of Purkinje cells onto CN neurons. MF, PF, and BS indicate mossy fibers, parallel fibers, and basket cell/stellate cells, respectively. (B) Measure for the spike probability of five IO neurons as a function of time. Two different situations are investigated: a synchronized IO, in which IO neurons activate collectively due to coupling (wild-types, blue), and an asynchronous IO, in which each neuron fires independently ($Cx36^{-/-}$ mutants, red). Wild-type curves all settle at the same equilibrium value P_{IO}^{∞}, while mutant curves remain above or below this value. (C) Phase plots of the average PF to PK synaptic strength S of five Purkinje cells. The derivative of S represents the plastic change of S at each time step due to synaptic plasticity. PF activity determines the *rate* at which plasticity occurs, while the *ratio* of depression versus potentiation depends on the frequency of climbing fiber activation. Synaptic strengths are stable when the derivative of S equals zero. (Top panel) A synchronous IO produces synchronous climbing fiber activation, such that all Purkinje cells share a common stable state. (Bottom panel) In an asynchronous IO, each neuron fires at its own specific rate, resulting in different depression versus potentiation ratios in each Purkinje cell. Thus, in this situation each individual Purkinje cell strives for a different state of the network in order to stabilize its synaptic strengths. (D) Development of synaptic strengths in time for a synchronous IO (blue) and an asynchronous IO (red). Wild-type Purkinje cells all receive the same stabilizing climbing fiber input, at which depression and potentiation exactly cancel each other over time. Their synaptic strengths therefore remain stable. $Cx36^{-/-}$ mutant Purkinje cells receive climbing fiber inputs that are either above or below equilibrium, resulting in too much depression or potentiation, respectively. Synapses therefore saturate at their minimum or maximum strengths. (E) Eye-blink responses of wild-types (blue) and $Cx36^{-/-}$ mutants (red) resulting from a real-time simulation of the architecture in panel (A). An additional plasticity rule was incorporated at the MF to CN synapse, allowing for the development of the "block" response in the CN. In wild-types, inhibitory input from the cortex modulates the "block" activity in the CN to produce a well-timed response. In $Cx36^{-/-}$ mutants, saturation of PF to PK synaptic strengths prevents induction and maintenance of the right levels of depression and potentiation, resulting in insufficient cortical modulation. Details are provided as Supplemental Data (part D).

Frisch et al., 2005). Here, we show that a lack of electrotonic coupling in the inferior olive leads to abnormal firing patterns of its neurons, which in turn can contribute to deficits in the timing of conditioned motor responses. The behavioral deficits in the global $Cx36^{-/-}$ mutants could be prominently revealed in different paradigms in which either a locomotion response or an eye-blink response was conditioned to a tone. In both cases, conditioned responses occurred, but the timing that had to be learned to make the response optimal was aberrant. In the locomotion test on the Erasmus ladder, $Cx36^{-/-}$ mutants were impaired in learning to avoid a bar that rose after a fixed period after the onset of the tone. Likewise, in the eye-blink test, the coupling-deficient mutants showed after four training sessions a mismatch in their latency to peak amplitude of ~200 ms with respect to the

onset of an air puff. This period stands in marked contrast to the 10–20 ms delay that can be observed in the basic eye movement responses of Cx36 null mutants to optokinetic stimulation (Kistler et al., 2002) or in the tremorgenic, limb, and body movements of coupling-deficient rats treated with replication-incompetent lentiviral vectors (Placantonakis et al., 2004). The behavioral deficits in learning-dependent timing in the *Cx36*$^{-/-}$ mutants were robust despite secondary compensations that may occur (De Zeeuw et al., 2003). Moreover, we observed the same type of deficits in the conditioning process following application of carbenoxolone and mefloquine, which are known to block olivary coupling in an acute fashion (Blenkinsop and Lang, 2006; Martin and Handforth, 2006; Placantonakis et al., 2006). Although one cannot rule out short-term compensations or side effects with this approach either (Rozental et al., 2001; Cruikshank et al., 2004), still the behavioral effects were significant and similar to those in the global mutants, while they cannot be due to the potential long-term compensations that may occur in the *Cx36*$^{-/-}$ mutants. Importantly, the effects of mefloquine could be readily observed after injection into the inferior olive itself, indicating that it is the coupling in the olive that is essential for learning-dependent timing of motor responses. These data in turn were supported by the finding that the abnormal timing of the conditioned eye-blink responses in the global *Cx36*$^{-/-}$ mutants was not observed in floxed Cx36 knockouts, in which Cx36 is normally expressed in the relevant olivary subnuclei, but not in most other Cx36-expressing neurons in the brain. Together, these findings indicate that the role of coupling between inferior olivary neurons becomes apparent when the olivocerebellar system is challenged in a cerebellar motor learning task and that it serves to facilitate learning-dependent timing in response to unexpected events rather than timing of movements per se.

In combination with modeling studies of both olivary neurons and the olivocerebellar system as a whole, our electrophysiological recordings demonstrated that a lack of precision in the timing of the climbing fiber responses mediating the US signals (present data) as well as a reduction in synchrony of climbing fiber activities during spontaneous activity (Marshall et al., 2007; but cf. Kistler et al., 2002) are probably responsible for the behavioral deficits in the coupling-deficient *Cx36*$^{-/-}$ mutants. The lack of precision in timing is due to increased variety in the responses after the US, which in turn probably results from altered interactions with the subthreshold oscillations in the inferior olive of *Cx36*$^{-/-}$ mutants. Our whole-cell recordings of olivary neurons in vivo did not only demonstrate that *Cx36*$^{-/-}$ mutants show less frequently subthreshold oscillations and that the stability of the remaining oscillations is reduced but also that the incidence of spikes occurring in the trough of these oscillations is significantly higher, while the correlation between their preferred spiking pattern and the frequency of their oscillations is generally weaker. The robust appearance of subthreshold oscillations of olivary neurons has recently also been shown in vivo in rats with the use of sharp electrode recordings (Chorev et al., 2007), while the contribution of electrotonic coupling to the occurrence of subthreshold oscillations in olivary cells has recently also been addressed in rats with the use of lentiviral knockdown of Cx36 or pharmacological blockage of gap junctions (Leznik and Llinas, 2005; Placantonakis et al., 2006). Thus, together with the current findings, we conclude that coupling supports the oscillations in the inferior olive in vivo and that the impact of oscillations on spiking patterns is reduced in uncoupled olivary neurons, which results in a more random timing of their spikes in relation to the oscillations.

The question remains as to how dynamic regulation of electrotonic coupling in the olive may contribute to learning-dependent timing (Llinas and Sasaki, 1989; De Zeeuw et al., 1998; Schweighofer et al., 1999; Bengtsson and Hesslow, 2006). Llinas and colleagues have provided strong evidence that the GABAergic input from the cerebellar nuclei, which terminates strategically at the coupled dendrites in olivary glomeruli (De Zeeuw et al., 1998), can uncouple the olivary neurons (Llinas and Sasaki, 1989; Lang et al., 1996). According to our model, such a mechanism would counteract learning-dependent timing of the conditioned responses, because it desynchronizes the climbing fiber inputs that mediate the signals of the US. Interestingly, Mauk and colleagues recently demonstrated that the GABAergic projection to the olive is necessary for extinction of the conditioned responses by reducing the firing rate of the relevant olivary neurons below resting level (Medina et al., 2002). Thus, in this respect, the mechanism of uncoupling and the mechanism of reducing the firing rate of olivary neurons may serve the same effect in that they both actively counteract the conditioning process.

EXPERIMENTAL PROCEDURES

Knockout Animals

Global *Cx36*$^{-/-}$ mutants and wild-type mice were generated and characterized as described by Guldenagel et al. (2001). The mutants that lacked Cx36 in their cerebellar nuclei neurons were cross-breedings of floxed-Cx36 mutants and parvalbumin-Cre mice. In contrast to the mouse published in Degen et al. (2004), the current conditional Cx36-deficient mouse has the 5′ loxP site inserted in the 5′UTR of Cx36 and not in the intron, leading to functional expression of the floxed Cx36 allele. Furthermore, after Cre-mediated deletion, a cyan fluorescent protein (CFP) was expressed instead of the floxed Cx36 allele (Figure 3B). Transfection of embryonic stem cells, creation of cell cultures, screening for cell clones, and injections of blastocysts were performed as described (Theis et al., 2000). Subsequently, Cx36+/flox(CFP) mice were mated to Cx36+/del (lacZ): parvalbumin-Cre mice to obtain cerebellum-deleted offspring with the genotype Cx36 del(lacZ)/flox(CFP): parvalbumin-Cre. For this study, we used offspring from a parvalbumin-Cre founder with multicopy integration of the transgene. All experiments were conducted in accordance with the European Communities Council Directive (86/609/EEC) and approved by the Dutch, British, and/or German national ethics committee.

Immunofluorescence

Cx36-/flox: parvalbumin-Cre mice and Cx36-/flox(CFP) littermate controls were anesthetized and perfused with 4% paraformaldehyde in PBS. The brains were removed and cut on a vibratome (Leica, UK), and the sections were immersed in rabbit anti-GFP (1:1000, Invitrogen, UK). Sections were washed in PBS and incubated in donkey anti-rabbit Cy3 (1:1000, Jackson ImmunoResearch, USA) prior to mounting (Vector Labs, UK). Cy3 was viewed with a custom filter set and Alexa 488 with FITC filters (Nikon E600 microscope), and images were captured directly from the slide using an Acquis Image Capture system (Synoptics, UK).

Erasmus Ladder

The Erasmus ladder is a fully automated system to screen both motor performance and motor learning capabilities of mutant mice in a noninvasive manner at a high-throughput level (for details see Supplemental Data section A). It consists of a horizontal ladder in between two shelter boxes, which are equipped

with two pressurized air outlets (Pneumax, 171E2B.T.A.0009) to control the moment of departure and speed of the mouse. The ladder has 2 × 37 rungs for the left and right side. All rungs are equipped with pressure sensors (produced at Erasmus MC), which are continuously monitored and which can be used to register and analyze the walking pattern of the mouse instantaneously. Moreover, based upon the prediction of the walking pattern, the rungs can be moved up or down by a high-speed pneumatic slide (Pneumax, 2141.52.00.36.91) with a maximum of 13 mm at any moment in time. The computer system (National Instruments, PXI-1000B) that runs the real-time system to record sensor data, adjust air pressure, predict future touches, calculate interventions, reposition slides, and store data operates in a fixed cycle of 2 ms. In the conditioning procedures, a 15 kHz tone (Voltcraft 7202), which gradually increases over 20 ms to 100 dB and which lasts up to 300 ms, was used as the CS, while a rising rung, which ascends 12 mm, was used as the US. The trials were separated by a random intertrial interval ranging from 8 to 12 s.

Pharmacological interventions were done with either carbenoxolone injections i.p. (40 mg/kg in 0.9% NaCl) or mefloquine injections into the olive (150 μM in 0.2% DMSO). Dosages were chosen so as to make sure that impact on coupling was warranted, while side effects were minimized (Blenkinsop and Lang, 2006; Cruikshank et al., 2004; Gareri et al., 2005; Margineanu and Klitgaard, 2006). Mice were anesthetized with ketamine/xylazine (80 mg/kg and 2 mg/kg), their atlanto-occipital membrane was opened, and the olive was identified electrophysiologically (Ruigrok and Voogd, 2000). Subsequently, the recording pipette was replaced by a pipette (tip diameter: 10–12 μm) filled with mefloquine and/or 2% BDA (Molecular Probes, Leiden, The Netherlands), and pressure injections of 50–100 nl were made within the olivary complex (see Figure 2C). After the conditioning sessions, the animals were anesthetized with an overdose of pentobarbital (200 mg/kg i.p.) and perfused with saline and paraformaldehyde (4% in phosphate buffer). The brains were collected, embedded in gelatin, cut at 40 μm transverse sections, and mounted (Ruigrok and Apps, 2007). In case of the BDA injections, sections were processed according to a BDA protocol using ABC-elite (Vector Laboratories) and DAB histochemistry (Pijpers et al., 2005).

Eye-Blink Conditioning

Wild-type and mutant mice were prepared for eye-blink conditioning according to the MDMT procedure (Koekkoek et al., 2002, 2005). Mice were subjected to either a paired or a randomly paired procedure; both procedures lasted 4 days, during each of which one session (64 trials grouped in 8 blocks) was conducted.

Extracellular Recordings

Mice were prepared by placing a recording chamber above the simplex lobule and adjacent areas. Extracellular Purkinje cell activities were recorded in the eye-blink region of awake animals with glass microelectrodes using a Multiclamp 700A and Digidata 1322A from Axon Instruments. Complex spike responses were recorded during 1 Hz air puff stimulation to the eye and analyzed off-line. A voltage threshold was used to detect complex spikes, and the time and waveform of the voltage records were used for off-line analysis (IGOR analysis software; WaveMetrics, OR).

Whole-Cell Recordings In Vivo

Mice were prepared for experiments under isoflurane or ketamine/xylazine anesthesia (for details see Khosrovani et al., 2007). Recordings were amplified with a MultiClamp 700A and DIGIDATA 1322A (Axon Instruments), and membrane potentials were corrected for junction potential (8 mV). In current-clamp experiments, we measured voltage responses to a series of negative current steps (100 pA). Correlations between the subthreshold oscillation frequencies and preferred spiking frequencies were determined by analyzing autocorrelograms (clampfit 9.0 software, Axon Instruments, CA). Bursts with a significant poisson surprise value (>5) were correlated to the corresponding subthreshold oscillation (STO) frequency extracted from the power spectrum of the recordings.

Simulations of Inferior Olive

The model used for the inferior olivary cell ensemble simulations was a modified version of a two-compartmental cell model by Schweighofer et al. (1999). The h current was moved to the dendritic compartment and redefined as:

$$q_\infty(V_d) = \frac{1}{1+\exp[(V_d+80)/4]}$$

$$\tau_q(V_d) = \frac{1}{\exp(-0.086V_d - 14.6) + \exp(0.07V_d - 1.87)}$$

with V_d as the dendritic membrane potential. Per cell type, five ensembles of neurons on a 5 × 5 grid were simulated. Wild-type cells were connected to all directly neighboring neurons (up to 8) with gap junction conductance set at 0.04 pS/cm^2. For the mutant model, Ca^{2+} conductances were increased as suggested by earlier research (De Zeeuw et al., 2003), with the new conductances for high- and low-threshold Ca^{2+} set at 4.4 pS/cm^2 and 1.3 pS/cm^2, respectively (a 10% increase compared to the wild-type values). Of the two depolarizing currents used, the first (4.5 μA/cm^2, 15 ms) was applied at 600 ± 10 ms after the start of the simulation, and the second (2.5 μA/cm^2, 15 ms) at 700 ± 10 ms. The exact timing was randomly determined per cell.

Model and Simulations of Olivocerebellar System

In the model, variable synaptic strengths are governed by coincidence rules for parallel fiber and climbing fiber activity probabilities. Synapses are accordingly described by differential equations, which are coupled by linear relations that represent the olivocerebellar loop. This formulation directly allows producing the phase plots shown in Figure 7C. The equations were solved by numerical integration using MATLAB's function *ode45*, which is a fourth-order Runge-Kutta solver. Resulting time-trajectory plots of synaptic strengths are shown in Figure 7D. The model equations were then implemented in real-time simulations running with a 5 ms time-step (performed in MATLAB). In these real-time simulations, inferior olivary neurons were simulated as spiking neurons. A training paradigm consisting of paired inputs representing conditioned stimulus and unconditioned stimulus was used to train the network, both in the case of synchronous and asynchronous inferior olive activity (Figure 7E). Further details on constraints, formulas, and simulations are presented in an extensive report in the Supplemental Data (section D).

SUPPLEMENTAL DATA

The Supplemental Data for this article can be found online at http://www.neuron.org/cgi/content/full/58/4/599/DC1/.

ACKNOWLEDGMENTS

We thank E. Dalm and J.v.d. Burg for their technical assistance, R. Maex for his advise on the model, and T.J.H. Ruigrok for help with the injections. The work in the group of C.I.D.Z. was supported by the Dutch Organization for Medical Sciences (ZON-MW), Life Sciences (NWO-ALW), Senter (Neuro-Bsik), Prinses Beatrix Fonds, and the European Community (EEC; SENSOPAC). Work in the Bonn laboratory was supported by the German Research Association (Wi 270/22-5,6) to K.W. Research of the H.M. team is supported by the Schilling Foundation.

Received: July 16, 2007
Revised: December 12, 2007
Accepted: March 9, 2008
Published: May 21, 2008

REFERENCES

Bengtsson, F., and Hesslow, G. (2006). Cerebellar control of the inferior olive. Cerebellum *5*, 7–14.

Bennett, M.V., and Zukin, R.S. (2004). Electrical coupling and neuronal synchronization in the Mammalian brain. Neuron *41*, 495–511.

Blenkinsop, T.A., and Lang, E.J. (2006). Block of inferior olive gap junctional coupling decreases Purkinje cell complex spike synchrony and rhythmicity. J. Neurosci. *26*, 1739–1748.

Buhl, D.L., Harris, K.D., Hormuzdi, S.G., Monyer, H., and Buzsaki, G. (2003). Selective impairment of hippocampal gamma oscillations in connexin-36 knock-out mouse in vivo. J. Neurosci. *23*, 1013–1018.

Bullock, T.H., Bennett, M.V., Johnston, D., Josephson, R., Marder, E., and Fields, R.D. (2005). Neuroscience. The neuron doctrine, redux. Science *310*, 791–793.

Chorev, E., Yarom, Y., and Lampl, I. (2007). Rhythmic episodes of subthreshold membrane potential oscillations in the rat inferior olive nuclei in vivo. J. Neurosci. *27*, 5043–5052.

Coesmans, M., Weber, J.T., De Zeeuw, C.I., and Hansel, C. (2004). Bidirectional parallel fiber plasticity in the cerebellum under climbing fiber control. Neuron *44*, 691–700.

Condorelli, D.F., Parenti, R., Spinella, F., Trovato Salinaro, A., Belluardo, N., Cardile, V., and Cicirata, F. (1998). Cloning of a new gap junction gene (Cx36) highly expressed in mammalian brain neurons. Eur. J. Neurosci. *10*, 1202–1208.

Connors, B.W., and Long, M.A. (2004). Electrical synapses in the mammalian brain. Annu. Rev. Neurosci. *27*, 393–418.

Cruikshank, S.J., Hopperstad, M., Younger, M., Connors, B.W., Spray, D.C., and Srinivas, M. (2004). Potent block of Cx36 and Cx50 gap junction channels by mefloquine. Proc. Natl. Acad. Sci. USA *101*, 12364–12369.

De Zeeuw, C.I., and Yeo, C.H. (2005). Time and tide in cerebellar memory formation. Curr. Opin. Neurobiol. *15*, 667–674.

De Zeeuw, C.I., Hertzberg, E.L., and Mugnaini, E. (1995). The dendritic lamellar body: a new neuronal organelle putatively associated with dendrodendritic gap junctions. J. Neurosci. *15*, 1587–1604.

De Zeeuw, C.I., Simpson, J.I., Hoogenraad, C.C., Galjart, N., Koekkoek, S.K., and Ruigrok, T.J. (1998). Microcircuitry and function of the inferior olive. Trends Neurosci. *21*, 391–400.

De Zeeuw, C.I., Chorev, E., Devor, A., Manor, Y., Van Der Giessen, R.S., De Jeu, M.T., Hoogenraad, C.C., Bijman, J., Ruigrok, T.J., French, P., et al. (2003). Deformation of network connectivity in the inferior olive of connexin 36-deficient mice is compensated by morphological and electrophysiological changes at the single neuron level. J. Neurosci. *23*, 4700–4711.

Deans, M.R., Gibson, J.R., Sellitto, C., Connors, B.W., and Paul, D.L. (2001). Synchronous activity of inhibitory networks in neocortex requires electrical synapses containing connexin36. Neuron *31*, 477–485.

Deans, M.R., Volgyi, B., Goodenough, D.A., Bloomfield, S.A., and Paul, D.L. (2002). Connexin36 is essential for transmission of rod-mediated visual signals in the mammalian retina. Neuron *36*, 703–712.

Degen, J., Meier, C., Van Der Giessen, R.S., Sohl, G., Petrasch-Parwez, E., Urschel, S., Dermietzel, R., Schilling, K., De Zeeuw, C.I., and Willecke, K. (2004). Expression pattern of lacZ reporter gene representing connexin36 in transgenic mice. J. Comp. Neurol. *473*, 511–525.

Frisch, C., De Souza-Silva, M.A., Sohl, G., Guldenagel, M., Willecke, K., Huston, J.P., and Dere, E. (2005). Stimulus complexity dependent memory impairment and changes in motor performance after deletion of the neuronal gap junction protein connexin36 in mice. Behav. Brain Res. *157*, 177–185.

Garcia, K.S., and Mauk, M.D. (1998). Pharmacological analysis of cerebellar contributions to the timing and expression of conditioned eyelid responses. Neuropharmacology *37*, 471–480.

Gareri, P., Condorelli, D., Belluardo, N., Citraro, R., Barresi, V., Trovato-Salinato, A., Mudò, G., Ibbadu, G.F., Russo, E., and De Sarro, G. (2005). Antiabsence effects of carbenoxolone in two genetic animal models of absence epilepsy (WAG/Rij rats and Ih/Ih mice). Neuropharmacology *49*, 551–563.

Guldenagel, M., Ammermuller, J., Feigenspan, A., Teubner, B., Degen, J., Sohl, G., Willecke, K., and Weiler, R. (2001). Visual transmission deficits in mice with targeted disruption of the gap junction gene connexin36. J. Neurosci. *21*, 6036–6044.

Hesslow, G. (1994). Correspondence between climbing fibre input and motor output in eyeblink-related areas in cat cerebellar cortex. J. Physiol. *476*, 229–244.

Hesslow, G., Svensson, P., and Ivarsson, M. (1999). Learned movements elicited by direct stimulation of cerebellar mossy fiber afferents. Neuron *24*, 179–185.

Kenyon, G.T., Medina, J.F., and Mauk, M.D. (1998). A mathematical model of the cerebellar-olivary system I: self-regulating equilibrium of climbing fiber activity. J. Comput. Neurosci. *5*, 17–33.

Kistler, W.M., De Jeu, M.T., Elgersma, Y., Van Der Giessen, R.S., Hensbroek, R., Luo, C., Koekkoek, S.K., Hoogenraad, C.C., Hamers, F.P., Gueldenagel, M., et al. (2002). Analysis of Cx36 knockout does not support tenet that olivary gap junctions are required for complex spike synchronization and normal motor performance. Ann. N Y Acad. Sci. *978*, 391–404.

Khosrovani, S., Van Der Giessen, R.S., De Zeeuw, C.I., and De Jeu, M.T. (2007). In vivo mouse inferior olive neurons exhibit heterogeneous subthreshold oscillations and spiking patterns. Proc. Natl. Acad. Sci. USA *104*, 15911–15916.

Koekkoek, S.K., Den Ouden, W.L., Perry, G., Highstein, S.M., and De Zeeuw, C.I. (2002). Monitoring kinetic and frequency-domain properties of eyelid responses in mice with magnetic distance measurement technique. J. Neurophysiol. *88*, 2124–2133.

Koekkoek, S.K., Hulscher, H.C., Dortland, B.R., Hensbroek, R.A., Elgersma, Y., Ruigrok, T.J., and De Zeeuw, C.I. (2003). Cerebellar LTD and learning-dependent timing of conditioned eyelid responses. Science *301*, 1736–1739.

Koekkoek, S.K., Yamaguchi, K., Milojkovic, B.A., Dortland, B.R., Ruigrok, T.J., Maex, R., De Graaf, W., Smit, A.E., VanderWerf, F., Bakker, C.E., et al. (2005). Deletion of FMR1 in Purkinje cells enhances parallel fiber LTD, enlarges spines, and attenuates cerebellar eyelid conditioning in Fragile X syndrome. Neuron *47*, 339–352.

Landisman, C.E., Long, M.A., Beierlein, M., Deans, M.R., Paul, D.L., and Connors, B.W. (2002). Electrical synapses in the thalamic reticular nucleus. J. Neurosci. *22*, 1002–1009.

Lang, E.J., Sugihara, I., and Llinas, R. (1996). GABAergic modulation of complex spike activity by the cerebellar nucleoolivary pathway in rat. J. Neurophysiol. *76*, 255–275.

Leznik, E., and Llinas, R. (2005). Role of gap junctions in synchronized neuronal oscillations in the inferior olive. J. Neurophysiol. *94*, 2447–2456.

Leznik, E., Makarenko, V., and Llinas, R. (2002). Electrotonically mediated oscillatory patterns in neuronal ensembles: an *in vitro* voltage-dependent dye-imaging study in the inferior olive. J. Neurosci. *22*, 2804–2815.

Llinas, R., and Yarom, Y. (1981). Electrophysiology of mammalian inferior olivary neurones *in vitro*. Different types of voltage-dependent ionic conductances. J. Physiol. *315*, 549–567.

Llinas, R., and Sasaki, K. (1989). The functional organization of the olivo-cerebellar system as examined by multiple purkinje cell recordings. Eur. J. Neurosci. *1*, 587–602.

Long, M.A., Deans, M.R., Paul, D.L., and Connors, B.W. (2002). Rhythmicity without synchrony in the electrically uncoupled inferior olive. J. Neurosci. *22*, 10898–10905.

Long, M.A., Jutras, M.J., Connors, B.W., and Burwell, R.D. (2005). Electrical synapses coordinate activity in the suprachiasmatic nucleus. Nat. Neurosci. *8*, 61–66.

Mann-Metzer, P., and Yarom, Y. (1999). Electrotonic coupling interacts with intrinsic properties to generate synchronized activity in cerebellar networks of inhibitory interneurons. J. Neurosci. *19*, 3298–3306.

Margineanu, D.G., and Klitgaard, H. (2006). The connexin 36 blockers quinine, quinidine and mefloquine inhibit cortical spreading depression in a rat neocortical slice model in vitro. Brain Res. Bull. *71*, 23–28.

Marshall, S.P., Van Der Giessen, R.S., De Zeeuw, C.I., and Lang, E.J. (2007). Altered olivocerebellar activity patterns in the connexin36 knockout mouse. Cerebellum *6*, 287–299.

Martin, F.C., and Handforth, A. (2006). Carbenoxolone and mefloquine suppress tremor in the harmaline mouse model of essential tremor. Mov. Disord. *21*, 1641–1649.

Mauk, M.D., and Donegan, N.H. (1997). A model of Pavlovian eyelid conditioning based on the synaptic organization of the cerebellum. Learn. Mem. *4*, 130–158.

Mauk, M.D., Steinmetz, J.E., and Thompson, R.F. (1986). Classical conditioning using stimulation of the inferior olive as the unconditioned stimulus. Proc. Natl. Acad. Sci. USA *83*, 5349–5353.

Medina, J.F., and Mauk, M.D. (2000). Computer simulation of cerebellar information processing. Nat. Neurosci. Suppl. *3*, 1205–1211.

Medina, J.F., Nores, W.L., and Mauk, M.D. (2002). Inhibition of climbing fibres is a signal for the extinction of conditioned eyelid responses. Nature *416*, 330–333.

Perrett, S.P., Ruiz, B.P., and Mauk, M.D. (1993). Cerebellar cortex lesions disrupt learning-dependent timing of conditioned eyelid responses. J. Neurosci. *13*, 1708–1718.

Pijpers, A., Voogd, J., and Ruigrok, T.J. (2005). Topography of olivo-corticonuclear modules in the intermediate cerebellum of the rat. J. Comp. Neurol. *492*, 193–213.

Placantonakis, D.G., Bukovsky, A.A., Zeng, X.H., Kiem, H.P., and Welsh, J.P. (2004). Fundamental role of inferior olive connexin 36 in muscle coherence during tremor. Proc. Natl. Acad. Sci. USA *101*, 7164–7169.

Placantonakis, D.G., Bukovsky, A.A., Aicher, S.A., Kiem, H.P., and Welsh, J.P. (2006). Continuous electrical oscillations emerge from a coupled network: a study of the inferior olive using lentiviral knockdown of connexin36. J. Neurosci. *26*, 5008–5016.

Porras-Garcia, E., Cendelin, J., Dominguez-del-Toro, E., Vozeh, F., and Delgado-Garcia, J.M. (2005). Purkinje cell loss affects differentially the execution, acquisition and prepulse inhibition of skeletal and facial motor responses in Lurcher mice. Eur. J. Neurosci. *21*, 979–988.

Raymond, J.L., Lisberger, S.G., and Mauk, M.D. (1996). The cerebellum: a neuronal learning machine? Science *272*, 1126–1131.

Rozental, R., Srinivas, M., and Spray, D.C. (2001). How to close a gap junction channel. Efficacies and potencies of uncoupling agents. Methods Mol. Biol. *154*, 447–476.

Ruigrok, T.J.H., and Voogd, J. (1995). Cerebellar influence on olivary excitability in the cat. Eur. J. Neurosci. *7*, 679–693.

Ruigrok, T.J., and Voogd, J. (2000). Organization of projections from the inferior olive to the cerebellar nuclei in the rat. J. Comp. Neurol. *426*, 209–228.

Ruigrok, T.J., and Apps, R. (2007). A light microscope-based double retrograde tracer strategy to chart central neuronal connections. Nat. Protocols *2*, 1869–1878.

Saffitz, J.E., Laing, J.G., and Yamada, K.A. (2000). Connexin expression and turnover: implications for cardiac excitability. Circ. Res. *86*, 723–728.

Schweighofer, N., Doya, K., and Kawato, M. (1999). Electrophysiological properties of inferior olive neurons: A compartmental model. J. Neurophysiol. *82*, 804–817.

Seto-Ohshima, A., Emson, P.C., Berchtold, M.W., and Heizmann, C.W. (1989). Localization of parvalbumin mRNA in rat brain by in situ hybridization histochemistry. Exp. Brain Res. *75*, 653–658.

Simpson, J.I., Wylie, D.R., and De Zeeuw, C.I. (1996). On climbing fiber signals and their consequences. Behav. Brain Sci. *19*, 380–395.

Sohl, G., Degen, J., Teubner, B., and Willecke, K. (1998). The murine gap junction gene connexin36 is highly expressed in mouse retina and regulated during brain development. FEBS Lett. *428*, 27–31.

Theis, M., Magin, T.M., Plum, A., and Willecke, K. (2000). General or cell type-specific deletion and replacement of connexin-coding DNA in the mouse. Methods *20*, 205–218.

Van Alphen, A.M., Schepers, T., Luo, C., and De Zeeuw, C.I. (2002). Motor performance and motor learning in Lurcher mice. Ann. N Y Acad. Sci. *978*, 413–424.

Van Der Giessen, R.S., Maxeiner, S., French, P.J., Willecke, K., and De Zeeuw, C.I. (2006). Spatiotemporal distribution of Connexin45 in the olivocerebellar system. J. Comp. Neurol. *495*, 173–184.

Voogd, J., and Glickstein, M. (1998). The anatomy of the cerebellum. Trends Neurosci. *21*, 370–375.

Wang, S.S., Denk, W., and Hausser, M. (2000). Coincidence detection in single dendritic spines mediated by calcium release. Nat. Neurosci. *3*, 1266–1273.